

On the size and shape of excluded volume polymers confined between parallel plates

Debasish Chaudhuri* and Bela Mulder†

FOM Institute AMOLF, Science Park 104, 1098XG Amsterdam, The Netherlands

(Dated: September 14, 2018)

A number of recent experiments have provided detailed observations of the configurations of long DNA strands under nano-to-micrometer sized confinement. We therefore revisit the problem of an excluded volume polymer chain confined between two parallel plates with varying plate separation. We show that the non-monotonic behavior of the overall size of the chain as a function of plate-separation, seen in computer simulations and reproduced by earlier theories, can already be predicted on the basis of scaling arguments. However, the behavior of the size in a plane parallel to the plates, a quantity observed in recent experiments, is predicted to be monotonic, in contrast to the experimental findings. We analyze this problem in depth with a mean-field approach that maps the confined polymer onto an anisotropic Gaussian chain, which allows the size of the polymer to be determined separately in the confined and unconfined directions. The theory allows the analytical construction of a smooth cross-over between the small plate-separation de Gennes regime and the large plate-separation Flory regime. The results show good agreement with Langevin dynamics simulations, and confirm the scaling predictions.

PACS numbers: 82.35.Lr, 36.20.Ey, 87.15.-v

I. INTRODUCTION

With the typical length scales in cells ranging from tens of nanometers to tens of microns, their polymeric constituents are often spatially constrained. Some of the prominent examples are the cytoskeletal filamentous protein aggregates microtubules and F-actin, which can have lengths up to tens of microns. Recent studies on microtubules in plant cells [1], DNA packaging in viral capsids [2], DNA segregation in bacterial cell division [3–6] focused on properties of biopolymers strongly influenced by confining geometries. This has naturally led to increased interest in understanding the physics of strongly confined polymers. Among all the polymeric constituents of cell, DNA with its relatively low bending stiffness in comparison to its extremely long length has a special place as it can under most circumstances be described as an classical excluded volume polymer [7]. Important examples of confined DNA are (i) chromosomal DNA that can have bare lengths up to centimeters trapped inside cell nucleus of size in the range of $1 - 10\mu\text{m}$, (ii) bacterial DNA of lengths between $0.1 - 100\mu\text{m}$ trapped within a small bacterial volume which for the case of E.coli is about $2\mu\text{m}$ long and $0.5\mu\text{m}$ in diameter, (iii) mitochondrial DNA of length about $5\mu\text{m}$ for human beings with the available mitochondrial size between $0.5 - 10\mu\text{m}$. The combined effects of confinement, self-avoidance and entropic forces act together in deciding the structure and properties of confined polymers.

A number of single molecule fluorescence microscopy studies have recently investigated the structure and dynamics of confined DNA trapped between parallel

plates [8–11] or within cylindrical geometries [12–14] with the confining dimensions typically of the order of, or smaller than, the bulk radius of gyration of the polymer. In particular Bonthuis et al. [10] have recently observed DNA confined to parallel-plate nanochannels, showing among others an interesting non-monotonic variation of the two-dimensional (2d) projected radius of gyration with the distance between channel walls.

Theoretical analyses of confined excluded volume chains already have a long history, encompassing a number of different techniques and approaches such as scaling theories [15, 16], renormalization group methods [17, 18], computer simulations [8, 19–22], and mean field theory [23]. The qualitative picture that emerges from these analyses is simple: With increased degree of confinement, the polymer size shrinks in the confining direction(s), and expands in the non-confined direction(s). The expansion in the non-confined directions is due to the excluded volume repulsion between different polymer segments. According to de Gennes’ scaling theory [15], this expansion in the strongly confined regime has a power-law dependence on the length-scale of the confinement. On the other hand, in the limit of very weak or no confinement the polymer is expected to behave as a free excluded volume polymer approximately obeying the Flory relationship between polymer length and spatial size in three dimensions (3d) [7].

Monte-Carlo (MC) simulations of self-avoiding lattice random walks trapped within reflecting walls have validated the de Gennes scaling predictions [19, 20]. These simulations also showed a non-monotonic variation of the mean size of the polymer, measured as the full 3d radius of gyration, as a function of the inter-wall separation [19]. This non-monotonicity in the radius of gyration was later also captured by a mean field theory (MFT) calculation [23]. However, the experiments reported in Ref. [10] found non-monotonicity in the projected 2d size of the

*Electronic address: chaudhuri@amolf.nl

†Electronic address: mulder@amolf.nl

polymer, rather than its 3d average. To correctly interpret these results we need a theoretical approach that explicitly allows us to consider the behavior of the polymer in the confined and non-confined directions separately.

Here we revisit the problem of an excluded volume polymer confined between two parallel plates with the latter desideratum in mind. By reviewing the extant scaling approaches, we show that the non-monotonicity of the 3d radius of gyration with plate-separation already follows from a scaling analysis if due care is given to the details of its application. We then construct a mean-field theory (MFT) for the confined polymer that goes beyond the existing theory, in that it explicitly takes into account the symmetry breaking induced by the confinement in the construction of the non-interacting reference polymer. This approach allows the analytical determination of the prefactors of the scaling relations in the limits of strong and weak confinement respectively. The results of this approach are then validated by an explicit off-lattice simulation of a confined polymer. Our main result is that the size of the polymer transverse to the confining direction, i.e., parallel to the confining planes, grows *monotonically* with decreasing separation between the plates. The non-monotonicity of the 3d radius of gyration therefore is due to the fact that, with decreasing plate-separation, initially the polymer-size in the confining direction decreases more rapidly than that it grows in the unconfined directions, and eventually the latter becomes dominant.

The paper consists of three main sections. We begin with by describing the existing scaling approaches in Sec. II. In Sec. III we present our variational MFT calculation and its predictions. In Sec. IV we describe the Langevin dynamics simulation scheme, and compare the results with our MFT predictions. Finally we conclude in Sec. V by summarizing our results and providing an outlook. A number of appendices collect some of the more technical material.

II. SCALING THEORIES

In this section, we briefly review the existing scaling theories for a polymer confined between parallel plates. We show that the non-monotonicity of the mean polymer size as a function of the plate separation, as observed in earlier simulations [19], is in fact intrinsic to de Gennes scaling predictions.

The first scaling theory of self-avoiding polymer behavior is due to Flory. Because of their simplicity Flory like arguments have been extended to other cases, e.g., semiflexible polymers [24]. Within Flory scaling theory the free energy of an excluded volume polymer in d -dimensions can be written as [25],

$$\beta F \sim \frac{R^2}{Nl^2} + l^d \frac{N^2}{R^d},$$

where R is the end-to-end distance of the polymer con-

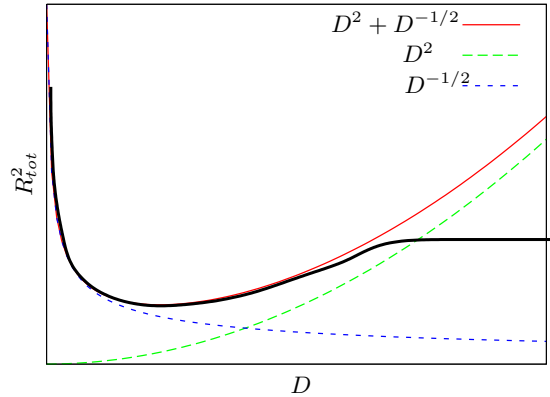


FIG. 1: (Color online) Schematic diagram of the non-monotonic behavior of average polymer size $R_{tot}^2 \sim a_1 D^2 + a_2 D^{-1/2}$ (dark thick line). In the limit of small D ($\lesssim L$ contour length), the combination of D^2 and $D^{-1/2}$ behavior of the polymer size in the confining and orthogonal directions, respectively, leads to non-monotonicity with a clear minimum in the average polymer size R_{tot}^2 . At large D ($> L$), R_{tot}^2 crosses over to the Flory regime and becomes independent of D .

structed of N segments, each of size l , $\beta = 1/k_B T$ with k_B the Boltzmann constant and T the ambient temperature. The first term describes the entropic elasticity of a free chain, and the second term describes the repulsive interaction between different segments. Minimizing the free energy with respect to R one obtains the Flory estimate of the equilibrium polymer size $R \sim N^{3/(d+2)} l$. As de Gennes pointed out [7], the success of Flory's theory relies on remarkable cancellation of overestimates in both the terms. For polymers confined between parallel plates, a Flory like argument predicts an equilibrium polymer-size in the unconfined directions that agrees with de Gennes scaling (which we discuss next), but the free energy it predicts is not extensive in N [22].

The de Gennes scaling arguments for the size of a polymer confined between parallel plates can be described as follows [15]. If the plate-separation $D \lesssim L = Nl$ the polymer contour length, the size of the polymer in the confining direction (perpendicular to the confining plates), R_{\perp} , becomes limited by the confinement, so that $R_{\perp} \sim D$. The size of the polymer in the unconfined directions (parallel to the confining plates), R_{\parallel} , should be entirely decided by the following two length scales: The 3d Flory size of a polymer $R \sim N^{3/5} l$, and the plate-separation D . Thus $R_{\parallel} = R \phi(R/D)$, so that $\phi(x) = 1$ when $x \rightarrow 0$ (3d Flory regime) and $\phi(x) \sim x^q$ when $x > 1$ (de Gennes regime). In the 2d-limit ($x \gg 1$) Flory scaling requires $R_{\parallel} \sim N^{3/4} l$. This ensures $q = 1/4$ and therefore $R_{\parallel} \sim N^{3/4} (l/D)^{1/4} l$. This power-law divergence of R_{\parallel} with decreasing D was observed in MC simulations of self-avoiding lattice random walks [19, 20], and also in recent experiments on confined DNA [10, 11]. The excess free energy measured from the state of an unconfined self-

avoiding polymer can be expressed [15] as $\beta F = \psi(R/D)$, so that $\psi(x) = 0$ for $x \rightarrow 0$ and $\psi(x) = x^p$ in the other limit of small D . Demanding that the excess free energy has to be an extensive function of N one obtains $p = 5/3$ and $\beta F \sim N(l/D)^{5/3}$.

We notice that, in terms of plate-separation D de Gennes scaling predicts two completely opposite behaviors for $R_{\perp} \sim D$ and $R_{\parallel} \sim N^{3/4}(l/D)^{1/4}l$. While R_{\perp} decreases, R_{\parallel} increases with decreasing D . Therefore, the mean size of the polymer, averaged over all the three directions, $R_{tot}^2 = R_{\perp}^2 + 2R_{\parallel}^2 \sim a_1 D^2 + a_2 D^{-1/2}$ (a_1, a_2 are positive constants) is expected to vary non-monotonically with D . The $R_{tot}^2 \sim D^{-1/2}$ behavior at very small D crosses over to $R_{tot}^2 \sim D^2$ at moderately large D via a minimum in R_{tot}^2 . This fact is illustrated in Fig. 1 and was observed in previous simulations [19]. At large D ($\gg L$), the scaling function $\phi(R/D) = 1$ and therefore the average size R_{tot}^2 becomes independent of D (Fig. 1). It should be noted here that this behavior is not the same as the non-monotonicity observed in experimental measurement of the parallel component of the radius of gyration of a DNA confined between parallel plates [10, 11]. de Gennes scaling predicts a clear monotonic increase of the component R_{\parallel} with shrinking D .

It is instructive to compare this behavior with that of an ideal chain confined between parallel plates. For an ideal chain, in absence of any interaction, the impact of the confinement remains restricted to the confining direction only. Thus $R_{\perp} \sim D$ for small D and $R_{\perp} \sim N^{1/2}l$ in the bulk limit. However, $R_{\parallel} \sim N^{1/2}l$ is obeyed independent of D . Therefore the overall size is $R_{tot}^2 \sim a_3 D^2 + 2R_{\parallel}^2$ with a_3 a positive constant. Starting from the bulk value, with shrinking D , R_{tot}^2 reduces to ultimately saturate at $2R_{\parallel}^2$. The initial reduction of overall size is thus common to both ideal polymers and excluded volume polymers. However, the expansion of the overall polymer size with further reduction of D for excluded volume polymers is a signature of the repulsion between polymer segments.

III. MEAN FIELD THEORY

A. Overview

The starting point for our MFT is a description of the polymer as a space curve $\mathbf{r}(s)$, in which s is the arc length parameter with domain $0 \leq s \leq L$. The energetics of the excluded volume (i.e., self-avoiding) polymer is given by the Edwards Hamiltonian [26]

$$\beta\mathcal{H} = \frac{3}{2l} \int_0^L ds \left(\frac{\partial \mathbf{r}(s)}{\partial s} \right)^2 + \frac{1}{2} b \int_0^L ds \int_0^L ds' \delta(\mathbf{r}(s) - \mathbf{r}(s')). \quad (1)$$

The parameter b sets the strength of the repulsive inter-segment interactions.

Edwards and Singh [26] first proposed to determine the size of a free self-avoiding polymer by mapping it onto an isotropic Gaussian chain with reference Hamiltonian

$$\beta\mathcal{H}_{\text{iso}} = \frac{3}{2l_0} \int_0^L ds \left(\frac{\partial \mathbf{r}(s)}{\partial s} \right)^2,$$

and then choosing the effective segment size l_0 self-consistently by requiring the first order variation of the mean-squared end-to-end distance $\langle R^2 \rangle$ in the interaction parameter b to vanish. This approach relatively simply reproduces the Flory result $R \sim N^{3/5}$ for the scaling of polymer size with polymer length. This same idea was later applied by Thirumalai and co-workers [23, 27] to confined polymers by first imposing the confinement on the isotropic Gaussian reference chain and then performing the self-consistent calculation of the effective segment length.

One can, however, pose the question whether an isotropic ideal reference chain is appropriate to the situation where the presence of the boundaries already explicitly breaks the bulk rotational symmetry. Here we propose to map the confined polymer onto an *anisotropic* reference chain, composed of bonds whose length depends on their absolute orientation with respect to the symmetry axes of the confining geometry. This anisotropic Gaussian reference-chain is described by the Hamiltonian

$$\beta\mathcal{H}_0 = \frac{3}{2l_{\parallel}} \int_0^L ds \left(\frac{\partial \mathbf{r}_{\parallel}(s)}{\partial s} \right)^2 + \frac{3}{2l_{\perp}} \int_0^L ds \left(\frac{\partial r_{\perp}(s)}{\partial s} \right)^2 \equiv \beta\mathcal{H}_{\parallel} + \beta\mathcal{H}_{\perp}. \quad (2)$$

The effective segment lengths l_{\parallel} and l_{\perp} are now the parameters that have to be determined self-consistently. Apart from the fact that this choice is physically plausible given the geometry of the system, it has two other potential advantages. It more explicitly yields independent predictions for the behavior of the polymer in the parallel and transverse directions with respect to the confinement, and generically multi-parameter mean field theories can be expected to yield better approximations to the underlying physics than single parameter ones.

We assume the z -axis of our coordinate system to be perpendicular to the confining planes. For convenience, we consider the lateral extent of the system to be finite, defined by a length $W \gg D$, but freely take the limit of an infinite extent wherever appropriate. The hard-wall confinement is implemented through the Dirichlet boundary condition by which the Green's function corresponding to the reference Hamiltonian vanishes at the two confining walls. The full Hamiltonian can be expressed as

$$\beta\mathcal{H} = \beta\mathcal{H}_0 + \beta\Delta\mathcal{H}_{\parallel} + \beta\Delta\mathcal{H}_{\perp} + \beta\Delta\mathcal{H}_b \quad (3)$$

where

$$\beta\Delta\mathcal{H}_{\parallel} = \frac{3}{2} \left(\frac{1}{l} - \frac{1}{l_{\parallel}} \right) \int_0^L ds \left(\frac{\partial \mathbf{r}_{\parallel}(s)}{\partial s} \right)^2, \quad (4)$$

$$\beta\Delta\mathcal{H}_{\perp} = \frac{3}{2} \left(\frac{1}{l} - \frac{1}{l_{\perp}} \right) \int_0^L ds \left(\frac{\partial r_{\perp}(s)}{\partial s} \right)^2, \quad (5)$$

$$\beta\Delta\mathcal{H}_b = \frac{1}{2} b \int_0^L ds \int_0^L ds' \delta(\mathbf{r}(s) - \mathbf{r}(s')) \quad (6)$$

are treated as perturbative corrections.

Statistical averages with respect to the Hamiltonian \mathcal{H} are defined through a path integral

$$\langle A[\mathbf{r}(s)] \rangle = \frac{1}{Z_{\mathcal{H}}} \int d\mathbf{r}(0) \int d\mathbf{r}(L) \int_{\mathbf{r}(0)}^{\mathbf{r}(L)} \mathcal{D}[\mathbf{r}(s)] A[\mathbf{r}(s)] \exp\{-\beta\mathcal{H}[\mathbf{r}(s)]\} \quad (7)$$

where the normalization constant is given by the partition function

$$Z_{\mathcal{H}} = \int d\mathbf{r}(0) \int d\mathbf{r}(L) \int_{\mathbf{r}(0)}^{\mathbf{r}(L)} \mathcal{D}[\mathbf{r}(s)] \exp\{-\beta\mathcal{H}[\mathbf{r}(s)]\}. \quad (8)$$

We now consider the components of the end-to-end separation $\mathbf{R}_{\parallel} = \mathbf{r}_{\parallel}(L) - \mathbf{r}_{\parallel}(0)$ and $R_{\perp} = r_{\perp}(L) - r_{\perp}(0)$ and the averages $\langle R_{\parallel}^2 \rangle$ and $\langle R_{\perp}^2 \rangle$. Expanding the Hamiltonian \mathcal{H} in the above expression up to linear order in $\Delta\mathcal{H}$ around the reference Hamiltonian \mathcal{H}_0 , we obtain

$$\langle R_{\parallel}^2 \rangle = \langle R_{\parallel}^2 \rangle_0 - \delta_{\parallel} + \mathcal{O}(\Delta\mathcal{H}^2), \quad (9)$$

$$\langle R_{\perp}^2 \rangle = \langle R_{\perp}^2 \rangle_0 - \delta_{\perp} + \mathcal{O}(\Delta\mathcal{H}^2) \quad (10)$$

where

$$\delta_{\parallel} = \left\{ \langle R_{\parallel}^2 \beta\Delta\mathcal{H}_{\parallel} \rangle_0 - \langle R_{\parallel}^2 \rangle_0 \langle \beta\Delta\mathcal{H}_{\parallel} \rangle_0 \right\} \quad (11)$$

$$+ \left\{ \langle R_{\parallel}^2 \beta\Delta\mathcal{H}_{\perp} \rangle_0 - \langle R_{\parallel}^2 \rangle_0 \langle \beta\Delta\mathcal{H}_{\perp} \rangle_0 \right\}$$

$$+ \left\{ \langle R_{\parallel}^2 \beta\Delta\mathcal{H}_b \rangle_0 - \langle R_{\parallel}^2 \rangle_0 \langle \beta\Delta\mathcal{H}_b \rangle_0 \right\}$$

$$\equiv \delta_{\parallel}^{\parallel} + \delta_{\parallel}^{\perp} + \delta_{\parallel}^b,$$

$$\delta_{\perp} = \left\{ \langle R_{\perp}^2 \beta\Delta\mathcal{H}_{\parallel} \rangle_0 - \langle R_{\perp}^2 \rangle_0 \langle \beta\Delta\mathcal{H}_{\parallel} \rangle_0 \right\} \quad (12)$$

$$+ \left\{ \langle R_{\perp}^2 \beta\Delta\mathcal{H}_{\perp} \rangle_0 - \langle R_{\perp}^2 \rangle_0 \langle \beta\Delta\mathcal{H}_{\perp} \rangle_0 \right\}$$

$$+ \left\{ \langle R_{\perp}^2 \beta\Delta\mathcal{H}_b \rangle_0 - \langle R_{\perp}^2 \rangle_0 \langle \beta\Delta\mathcal{H}_b \rangle_0 \right\}$$

$$\equiv \delta_{\perp}^{\parallel} + \delta_{\perp}^{\perp} + \delta_{\perp}^b.$$

$\langle \dots \rangle_0$ indicates a statistical average taken with respect to the reference Hamiltonian \mathcal{H}_0 . In the above expressions, $\delta_{\parallel}^{\parallel}$, $\delta_{\parallel}^{\perp}$, $\delta_{\perp}^{\parallel}$ and δ_{\perp}^{\perp} are the corrections due to the chain anisotropy, and δ_{\parallel}^b and δ_{\perp}^b are the corrections from excluded volume interactions. The MFT approximation requires a choice of l_{\parallel} and l_{\perp} so that $\langle R_{\parallel}^2 \rangle = \langle R_{\parallel}^2 \rangle_0$ and $\langle R_{\perp}^2 \rangle = \langle R_{\perp}^2 \rangle_0$. Thus, solving $\delta_{\parallel} = \delta_{\perp} = 0$, one can obtain the effective segment lengths l_{\parallel} and l_{\perp} in terms of

plate-separation D , contour length L and inter-segment interaction strength b .

Ref. [26] obtained Flory scaling within corrections up to linear order in $\beta\Delta\mathcal{H}$. The inclusion of higher order terms was shown to change the coefficients of scaling form, however, keeping them stable [26]. We expect the same to hold in the present problem as well [23], as the nature of interactions used here is exactly the same.

We now briefly summarize the main results we obtained using this MFT. In the limit of very large plate-separations ($D \rightarrow \infty$) the system becomes isotropic with

$$l_{\parallel} = l_{\perp} \equiv l_B \sim (bl)^{2/5} L^{1/5} \quad (13)$$

and the mean squared end-to-end separation follows the relation

$$\langle R^2 \rangle = Ll_B \sim (bl)^{2/5} L^{6/5} \quad (14)$$

which is independent of D and obeys Flory scaling.

In the limit of strong confinement ($D \rightarrow 0$),

$$l_{\perp} \simeq \frac{l}{2} \left(1 + \sqrt{1 - \frac{4bD}{ll_{\parallel}}} \right) \simeq l - \frac{4\sqrt{2\pi}}{3} \sqrt{\frac{b}{l}} \frac{D^{3/2}}{L^{1/2}} \quad (15)$$

$$l_{\parallel} \simeq \frac{l}{2} \left(1 + \sqrt{1 + \frac{9b}{2\pi l D}} \right) \simeq \frac{3}{2\sqrt{2\pi}} \sqrt{bl} \sqrt{\frac{L}{D}}. \quad (16)$$

Using these, we obtain the size of the polymer in the confining direction

$$\langle R_{\perp}^2 \rangle \simeq \left(1 - \frac{8}{\pi^2} \right) \frac{D^2}{2} - \frac{D^2}{8} e^{-3\kappa L} \quad (17)$$

with $\kappa = (1/6)l_{\perp}(\pi/D)^2$, and in the unconfined directions

$$\begin{aligned} \langle R_{\parallel}^2 \rangle &\simeq \frac{1}{3} Ll \left(1 + \sqrt{1 + \frac{9b}{2\pi l D}} \right) \\ &\sim \sqrt{\frac{1}{2\pi}} (bl)^{1/2} L^{3/2} D^{-1/2}. \end{aligned} \quad (18)$$

With shrinking plate-separation D the polymer gets compressed in the confining direction and expands in the free directions. Up to the leading order (in the small D limit) $\langle R_{\perp}^2 \rangle \sim D^2$ and $\langle R_{\parallel}^2 \rangle \sim L^{3/2} D^{-1/2}$ obeying de Gennes scaling. Beyond the leading order, the expressions we found describe a smooth crossover to large D behavior (see Fig. 2).

We now present a detailed derivation of the Eqs. 13 – 18.

B. Formulation

1. Green's function

In order to determine all the above mentioned averages, we require the Green's function corresponding to the anisotropic reference Hamiltonian \mathcal{H}_0 [Eq. (2)] defined as

$$G_0(\mathbf{r}, L | \mathbf{r}', 0) = \int_{\mathbf{r}'=\mathbf{r}(0)}^{\mathbf{r}=\mathbf{r}(L)} \mathcal{D}[\mathbf{r}(s)] \exp\{-\beta \mathcal{H}_0[\mathbf{r}(s)]\}. \quad (19)$$

The Green's function obeys the following differential equation [28],

$$\left(\frac{\partial}{\partial L} - \frac{l_{\parallel}}{6} \nabla_{\parallel}^2 - \frac{l_{\perp}}{6} \frac{d^2}{dz^2} \right) G_0 = 0. \quad (20)$$

Using the Dirichlet boundary condition in the confining direction $G_0(z=0, D) = 0$ and free boundary condition in the unconfined directions (along x and y axes), one obtains a variable separable form of the Green's function (see Appendix-A)

$$G_0 = G_{\parallel}(\mathbf{r}_{\parallel}, L | \mathbf{r}'_{\parallel}, 0) G_{\perp}(r_{\perp}, L | r'_{\perp}, 0) \quad (21)$$

where,

$$G_{\parallel} = \frac{3}{2\pi l_{\parallel} L} e^{-\frac{3}{2l_{\parallel} L} (\mathbf{r}_{\parallel} - \mathbf{r}'_{\parallel})^2}, \quad (22)$$

and

$$G_{\perp} = \frac{2}{D} \sum_{n=1}^{\infty} \sin\left(\frac{n\pi}{D} r_{\perp}\right) \sin\left(\frac{n\pi}{D} r'_{\perp}\right) e^{-\kappa n^2 L}, \quad (23)$$

with $\kappa = \frac{1}{6} l_{\perp} \left(\frac{\pi}{D}\right)^2$.

2. Partition function

The partition function corresponding to the reference Hamiltonian \mathcal{H}_0 can also be written in a variable-separable form

$$Z = \int d\mathbf{r}(\mathbf{L}) \int d\mathbf{r}(\mathbf{0}) \mathbf{G}_0(\mathbf{r}(\mathbf{L}), \mathbf{L} | \mathbf{r}(\mathbf{0}), \mathbf{0}) = \mathbf{Z}_{\parallel} \mathbf{Z}_{\perp} \quad (24)$$

where

$$Z_{\parallel} = \int d\mathbf{r}_{\parallel} \int d\mathbf{r}'_{\parallel} G_{\parallel}(\mathbf{r}_{\parallel}, L | \mathbf{r}'_{\parallel}, 0) = W^2 \quad (25)$$

and

$$\begin{aligned} Z_{\perp} &= \int dr_{\perp} \int dr'_{\perp} G_{\perp}(r_{\perp}, L | r'_{\perp}, 0) \\ &= \sum_{n=0}^{\infty} \frac{8D}{(2n+1)^2 \pi^2} e^{-\kappa L (2n+1)^2}. \end{aligned} \quad (26)$$

Remember that W^2 denotes the area of the unconfined xy -plane, and we freely take the limit $W \rightarrow \infty$ wherever appropriate.

3. End-to-end separation: Contribution from reference Hamiltonian

Using the above mentioned Green's function G_0 one can calculate the end-to-end separations

$$\begin{aligned} \langle R_{\parallel}^2 \rangle_0 &= \frac{\int d\mathbf{r}_{\parallel} \int d\mathbf{r}'_{\parallel} (\mathbf{r}_{\parallel} - \mathbf{r}'_{\parallel})^2 G_{\parallel}(\mathbf{r}_{\parallel}, L | \mathbf{r}'_{\parallel}, 0)}{\int d\mathbf{r}_{\parallel} \int d\mathbf{r}'_{\parallel} G_{\parallel}(\mathbf{r}_{\parallel}, L | \mathbf{r}'_{\parallel}, 0)} \\ &= \frac{2}{3} l_{\parallel} L \end{aligned} \quad (27)$$

and

$$\begin{aligned} \langle R_{\perp}^2 \rangle_0 &= \frac{\int_0^D dr_{\perp} \int_0^D dr'_{\perp} (r_{\perp} - r'_{\perp})^2 G_{\perp}(r_{\perp}, L | r'_{\perp}, 0)}{\int_0^D dr_{\perp} \int_0^D dr'_{\perp} G_{\perp}(r_{\perp}, L | r'_{\perp}, 0)} \\ &= \frac{D^2 \nu}{2 \xi} \end{aligned} \quad (28)$$

where,

$$\begin{aligned} \nu &= \sum_{n=0}^{\infty} \frac{1}{(2n+1)^2} \left(1 - \frac{8}{(2n+1)^2 \pi^2} \right) e^{-\kappa (2n+1)^2 L} \\ &\quad - \sum_{n=1}^{\infty} \frac{1}{(2n)^2} e^{-\kappa (2n)^2 L}, \end{aligned} \quad (29)$$

and

$$\xi = \sum_{n=0}^{\infty} \frac{1}{(2n+1)^2} e^{-\kappa (2n+1)^2 L}. \quad (30)$$

4. End-to-end separation: Corrections from chain anisotropy

We now calculate the first order contributions $\delta_{\parallel}^{\parallel}$, $\delta_{\parallel}^{\perp}$, $\delta_{\perp}^{\parallel}$ and δ_{\perp}^{\perp} that are due to the anisotropy of the reference chain. Using the definition of the mean-squared end-to-end distance

$$\langle R_{\parallel}^2 \rangle_0 = \frac{\int d\mathbf{r}_{\parallel} \int d\mathbf{r}'_{\parallel} \left(\mathbf{r}_{\parallel} - \mathbf{r}'_{\parallel} \right)^2 \int_{\mathbf{r}'_{\parallel}=\mathbf{r}_{\parallel}(0)}^{\mathbf{r}_{\parallel}=\mathbf{r}_{\parallel}(L)} \mathcal{D}[\mathbf{r}_{\parallel}(s)] \exp \left\{ -\beta \mathcal{H}_{\parallel}[\mathbf{r}(s)] \right\}}{\int d\mathbf{r}_{\parallel} \int d\mathbf{r}'_{\parallel} \int_{\mathbf{r}'_{\parallel}=\mathbf{r}_{\parallel}(0)}^{\mathbf{r}_{\parallel}=\mathbf{r}_{\parallel}(L)} \mathcal{D}[\mathbf{r}_{\parallel}(s)] \exp \left\{ -\beta \mathcal{H}_{\parallel}[\mathbf{r}(s)] \right\}}$$

along with the identity

$$\beta \mathcal{H}_{\parallel}[\mathbf{r}(s)] = \alpha_{\parallel} \frac{2}{3} \left(\frac{1}{l} - \frac{1}{l_{\parallel}} \right)^{-1} \beta \Delta \mathcal{H}_{\parallel}[\mathbf{r}(s)],$$

where $\alpha_{\parallel} = 3/2l_{\parallel}$, we obtain

$$\begin{aligned} & -\frac{3}{2} \left(\frac{1}{l} - \frac{1}{l_{\parallel}} \right) \frac{\partial}{\partial \alpha_{\parallel}} \langle R_{\parallel}^2 \rangle_0 \\ & = \left\{ \langle R_{\parallel}^2 \beta \Delta \mathcal{H}_{\parallel} \rangle_0 - \langle R_{\parallel}^2 \rangle_0 \langle \beta \Delta \mathcal{H}_{\parallel} \rangle_0 \right\} \\ \text{or, } \delta_{\parallel}^{\parallel} & = \frac{2}{3} \left(\frac{1}{l} - \frac{1}{l_{\parallel}} \right) L l_{\parallel}^2. \end{aligned} \quad (31)$$

Similarly, one can show that (with $\alpha_{\perp} = 3/2l_{\perp}$),

$$\delta_{\parallel}^{\perp} = -\frac{3}{2} \left(\frac{1}{l} - \frac{1}{l_{\perp}} \right) \frac{\partial}{\partial \alpha_{\perp}} \langle R_{\parallel}^2 \rangle_0 = 0 \quad (32)$$

$$\delta_{\perp}^{\parallel} = -\frac{3}{2} \left(\frac{1}{l} - \frac{1}{l_{\parallel}} \right) \frac{\partial}{\partial \alpha_{\parallel}} \langle R_{\perp}^2 \rangle_0 = 0 \quad (33)$$

$$\delta_{\perp}^{\perp} = -\frac{3}{2} \left(\frac{1}{l} - \frac{1}{l_{\perp}} \right) \frac{\partial}{\partial \alpha_{\perp}} \langle R_{\perp}^2 \rangle_0 \quad (34)$$

where the last derivative can be explicitly evaluated by considering Eq. (28). This leads to the following expression,

$$\begin{aligned} \delta_{\perp}^{\perp} & = -\frac{\pi^2}{12\xi} l_{\perp}^2 L \left(\frac{1}{l} - \frac{1}{l_{\perp}} \right) \\ & \times \left[\sum_{n=0}^{\infty} \left(1 - \frac{8}{(2n+1)^2 \pi^2} - \frac{\nu}{\xi} \right) e^{-\kappa L (2n+1)^2} \right. \\ & \left. - \sum_{n=1}^{\infty} e^{-\kappa L (2n)^2} \right] \end{aligned} \quad (35)$$

where ν and ξ are defined by Eq. (29) and Eq. (30) respectively.

5. End-to-end separation: Corrections from excluded volume interactions

Now we evaluate δ_{\parallel}^b and δ_{\perp}^b . Note that the presence of $\delta(\mathbf{r}(\mathbf{s}) - \mathbf{r}(\mathbf{s}'))$ in the self-avoidance interaction $\beta \Delta \mathcal{H}_b$ [Eq. (6)] couples the transverse and the longitudinal modes of the Green's function. This is the term through which $\langle R_{\parallel}^2 \rangle$ becomes dependent on the plate-separation D .

The calculation of these two terms are lengthy but straightforward. Here, we only quote the final results deferring the details of the calculations to Appendix-B:

$$\begin{aligned} \delta_{\parallel}^b & = -Z^{-1} \frac{b}{\pi} W^2 \sum_{n_L, n', n_0=1}^{\infty} M(n_L, n', n_0; \kappa) \\ & \times \left[2\delta_{n_0, n_L} + \delta_{n', (n_0+n_L)/2} - \delta_{n', (n_0-n_L)/2} \right. \\ & \left. - \delta_{n', (n_L-n_0)/2} \right] \times J_0(n_L, n_0) \end{aligned} \quad (36)$$

where,

$$M(n_L, n', n_0; \kappa) = e^{-\kappa L n_L^2} \times \int_0^L ds' \int_{s'}^L ds \left[e^{-\kappa s(n'^2 - n_L^2)} e^{-\kappa s'(n_0^2 - n'^2)} \right], \quad (37)$$

$$J_0(n_L, n_0) = \frac{1}{n_0 n_L \pi^2} [1 - (-1)^{n_L}] [1 - (-1)^{n_0}]; \quad (38)$$

and

$$\begin{aligned} \delta_{\perp}^b & = \frac{b}{Z} W^2 \frac{3}{2\pi l_{\parallel}} \sum_{n_L, n', n_0=1}^{\infty} D^2 K(n_L, n', n_0; \kappa) \\ & \times \left[2\delta_{n_0, n_L} + \delta_{n', (n_0+n_L)/2} \right. \\ & \left. - \delta_{n', (n_0-n_L)/2} - \delta_{n', (n_L-n_0)/2} \right] \\ & \times \left[J(n_L, n_0) - \frac{\langle R_{\perp}^2 \rangle_0}{D^2} J_0(n_L, n_0) \right] \end{aligned} \quad (39)$$

where,

$$K(n_L, n', n_0; \kappa) = e^{-\kappa L n_L^2} \lim_{a \rightarrow 0} \int_0^L ds' \int_{s'}^L ds \left[\frac{e^{-\kappa s(n'^2 - n_L^2)} e^{-\kappa s'(n_0^2 - n'^2)}}{(s - s') + a} \right] \quad (40)$$

$$\begin{aligned} J(n_L, n_0) & = -\frac{1}{n_L^3 n_0 \pi^4} [(-1)^{n_L} n_L^2 \pi^2 + 2(1 - (-1)^{n_L})] \\ & \times [1 - (-1)^{n_0}] - \frac{2}{n_L n_0 \pi^2} (-1)^{n_0} (-1)^{n_L} \\ & - \frac{1}{n_L n_0^3 \pi^4} [(-1)^{n_0} n_0^2 \pi^2 + 2(1 - (-1)^{n_0})] \\ & \times [1 - (-1)^{n_L}]. \end{aligned} \quad (41)$$

C. Results

1. Large plate-separation limit: $D \rightarrow \infty$

Here we demonstrate that the MFT scheme naturally leads to Flory scaling in the bulk limit of $D \rightarrow \infty$. This

limit is better appreciated, in a shifted coordinate system in which the confining hard walls are at $z = \pm D/2$. In this coordinate system, the transverse component of Green's function is,

$$G_{\perp} = \frac{1}{D} \sum_{n, \text{ even}} \sin \frac{n\pi z'}{D} \sin \frac{n\pi z}{D} e^{-\kappa n^2 L} + \frac{1}{D} \sum_{n, \text{ odd}} \cos \frac{n\pi z'}{D} \cos \frac{n\pi z}{D} e^{-\kappa n^2 L}.$$

In the continuum limit of $D \rightarrow \infty$

$$G_{\perp} = \sqrt{\frac{3}{2\pi l_{\perp} L}} \exp\left(-\frac{3}{2} \frac{(z - z')^2}{l_{\perp} L}\right). \quad (42)$$

$\delta_{\parallel}^{\parallel}$ is independent of D and is given by Eq. 31. The details of the calculation of δ_{\parallel}^b , δ_{\perp}^b and δ_{\perp}^{\perp} in this bulk limit are presented in Appendix-C. In this limit the equations, $\delta_{\parallel} = \delta_{\parallel}^{\parallel} + \delta_{\parallel}^b = 0$ and $\delta_{\perp} = \delta_{\perp}^{\perp} + \delta_{\perp}^b = 0$ imply,

$$\frac{Ll_{\parallel}^2}{l} \sim \frac{b}{l_{\perp}^{1/2}} L^{3/2} \quad (43)$$

and

$$\frac{Ll_{\perp}^2}{l} \sim \frac{bl_{\perp}^{1/2}}{l_{\parallel}} L^{3/2} \quad (44)$$

respectively. Eq. (43) and Eq. (44) leads to $l_{\parallel} = l_{\perp} \equiv l_B$, the isotropy expected in the limit of $D \rightarrow \infty$. This also implies

$$l_B \sim (bl)^{2/5} L^{1/5}. \quad (45)$$

and

$$\langle R^2 \rangle = Ll_B \sim (bl)^{2/5} L^{6/5}, \quad (46)$$

i.e., Flory scaling in three dimensions.

2. Narrow plate-separation limit: $D \rightarrow 0$

In the limit of $D \rightarrow 0$, $\kappa = l_{\perp}(\pi/D)^2/6 \rightarrow \infty$ and only the small n eigenfunctions contribute to the calculation of perturbative corrections to end-to-end distance. The simplest approximation in this limit is the ground state approximation (only the minimum value of n 's contribute).

Ground state approximation: We first calculate δ_{\parallel}^b within the ground state approximation. Using $n_0 = n' = n_L = 1$, we get $M(1, 1, 1; \kappa) = (L^2/2) \exp(-\kappa L)$ and $Z = W^2(8D/\pi^2) \exp(-\kappa L)$ which leads to $\delta_{\parallel}^b = -(3b/4\pi)(L^2/D)$ (using Eq. 36). Within MFT, l_{\parallel} satisfies the condition $\delta_{\parallel} = \delta_{\parallel}^{\parallel} + \delta_{\parallel}^b = 0$, which implies that,

$$\frac{2}{3} \left(\frac{1}{l} - \frac{1}{l_{\parallel}} \right) Ll_{\parallel}^2 = \frac{3b}{4\pi} \frac{L^2}{D}.$$

The solution of this equation gives

$$l_{\parallel} = \frac{l}{2} \left(1 + \sqrt{1 + \frac{9b}{2\pi l} \frac{L}{D}} \right),$$

which is Eq. 16. Therefore, we find the relation given in Eq. 18

$$\begin{aligned} \langle R_{\parallel}^2 \rangle &= \frac{2}{3} l_{\parallel} L = \frac{1}{3} Ll \left(1 + \sqrt{1 + \frac{9b}{2\pi l} \frac{L}{D}} \right) \\ &\sim \sqrt{\frac{1}{2\pi}} (bl)^{1/2} L^{3/2} D^{-1/2}. \end{aligned}$$

In the last step, the diverging part of $\langle R_{\parallel}^2 \rangle_0$ in the limit of $D \rightarrow 0$ is extracted. Thus, up to the leading order in the limit of $D \rightarrow 0$ we find de Gennes scaling $R_{\parallel} = \sqrt{\langle R_{\parallel}^2 \rangle} \sim (1/\sqrt{2\pi})(bl)^{1/4} L^{3/4} D^{-1/4}$.

Now we calculate the perpendicular component $\langle R_{\perp}^2 \rangle$ within the ground state approximation $n_L = n' = n_0 = 1$. Thus Eq. 39 reduces to

$$\delta_{\perp}^b = \frac{9b}{2\pi l_{\parallel} Z} W^2 D^2 K(1, 1, 1; \kappa) \left[J(1, 1) - \frac{4}{\pi^2} \frac{\langle R_{\perp}^2 \rangle_0}{D^2} \right].$$

In the expression of $\langle R_{\perp}^2 \rangle_0$ [Eq. (28)] we retain only the $n = 0$ terms, within the ground state approximation, to obtain $\langle R_{\perp}^2 \rangle_0 = 1 - 8/\pi^2$. This leads to $J(1, 1) - (4/\pi^2)\langle R_{\perp}^2 \rangle_0 = 0$ and therefore, $\delta_{\perp}^b = 0$. It can be easily seen that within the ground state approximation $\delta_{\perp}^{\perp} = 0$ too. Thus l_{\perp} remains indeterminate. We need to go up to the first excited state approximation (next higher values of n), to obtain the expression for l_{\perp} .

First excited state approximation: Within this approximation, we can write Eq. 39 as

$$\begin{aligned} \delta_{\perp}^b &= \frac{3b}{2\pi l_{\parallel} Z} W^2 D^2 [3K(1, 1, 1; \kappa) T_1 + 2K(1, 2, 1; \kappa) T_1 \\ &\quad + 2K(2, 1, 2; \kappa) T_2 + 3K(2, 2, 2; \kappa) T_2] \end{aligned}$$

where,

$$\begin{aligned} T_1 &= J(1, 1) - \frac{\langle R_{\perp}^2 \rangle_0}{D^2} J_0(1, 1) = \frac{1}{2\pi^2} e^{-3\kappa L}, \\ T_2 &= J(2, 2) - \frac{\langle R_{\perp}^2 \rangle_0}{D^2} J_0(2, 2) = -\frac{1}{2\pi^2}. \end{aligned}$$

We find,

$$K(1, 1, 1; \kappa) \simeq L e^{-\kappa L} \left[\log \left(\frac{L}{a} \right) - 1 \right].$$

We observe that the leading order behavior of $K(1, 1, 1; \kappa) \sim L \exp(-\kappa L)$ apart from a weak logarithmic divergence coming from the δ -function nature of the inter-segment repulsion ($a \rightarrow 0$). Therefore, $K(1, 1, 1; \kappa) T_1 \sim L \exp(-4\kappa L)$. Similarly one can show that all the terms in the above expression of δ_{\perp}^b has the same leading order behavior. Using $Z = W^2(8D/\pi^2) \exp(-\kappa L)$ we find that, $\delta_{\perp}^b \sim (bLD/l_{\parallel}) \exp(-3\kappa L)$.

Within the first excited state approximation, we can write Eq. 35 as

$$\delta_{\perp}^{\pm} = \frac{\pi^2}{16} e^{-3\kappa L} l_{\perp}^2 L \left(\frac{1}{l_{\perp}} - \frac{1}{l} \right).$$

Thus the mean field condition, $\delta_{\perp} = \delta_{\perp}^{\pm} + \delta_{\perp}^b = 0$ implies,

$$l_{\perp} \simeq \frac{l}{2} \left[1 + \sqrt{1 - \frac{4bD}{ll_{\parallel}}} \right]$$

which is Eq. 15. In the limit of $D \rightarrow 0$ we can write $l_{\perp} \simeq l - 2bD/l_{\parallel} \simeq l - (4\sqrt{2\pi}/3)\sqrt{b/l}D^{3/2}L^{-1/2}$. Thus the leading order behavior is $l_{\perp} \sim l$ with correction vanishing as $D^{3/2}$. Using this l_{\perp} in $\kappa = (1/6)l_{\perp}(\pi/D)^2$, we find

$$\langle R_{\perp}^2 \rangle \simeq \frac{D^2}{2} \left[\left(1 - \frac{8}{\pi^2} \right) \right] - \frac{D^2}{8} e^{-3\kappa L},$$

which is Eq. 17. The above expression means that, the leading order behavior (at smallest D values) of

$$\langle R_{\perp}^2 \rangle = \frac{D^2}{2} \left[\left(1 - \frac{8}{\pi^2} \right) \right]$$

has corrections in the next order (at larger D), which has a complicated functional dependence on inter-segment interaction strength b , plate-separation D and polymer contour-length L .

Before ending this section, we briefly discuss the pure 2d limit of the above-mentioned calculation. Variational MFT calculation for pure 2d leads to the mean squared end-to-end distance

$$\langle R_{2d}^2 \rangle \sim (b_0 l)^{1/2} L^{3/2}, \quad (47)$$

which obeys 2d Flory scaling. In the above expression b_0 measures the strength of the inter-segment repulsion and is dimensionless, in contrast to the same parameter in 3d denoted by b which has the dimension of length. This indicates that l is the only intrinsic microscopic length scale in the system. Requiring $b = b_0 l$, we find that $\langle R_{\parallel}^2 \rangle$ reaches the 2d limit of $\langle R_{2d}^2 \rangle$ when $D \sim l$ (see Appendix-D).

3. Non-monotonicity in overall polymer-size: Crossover

Clearly, the mean squared end-to-end distance $\langle R_{\text{tot}}^2 \rangle = 2\langle R_{\parallel}^2 \rangle + \langle R_{\perp}^2 \rangle$ should show a minimum as a function of changing plate-separation D . This comes about, because of the completely opposing behaviors of the two components – while the size in the confining direction $\langle R_{\perp}^2 \rangle$ shrinks with decreasing D , the polymer-size in the unconfined directions $\langle R_{\parallel}^2 \rangle$ expand. Keeping up to the leading order behavior in $\langle R_{\perp}^2 \rangle [= (1 - 8/\pi^2)D^2/2]$ one can easily find the cross-over plate-separation (using Eqs. 17 and 18)

$$D_c = (2\pi)^{-1/5} \left(1 - \frac{8}{\pi^2} \right)^{-2/5} (bl)^{1/5} L^{3/5} \quad (48)$$

where $\langle R_{\text{tot}}^2 \rangle$ reaches the minimum. With enhanced degree of confinement (reduced D) the total size of the polymer $\langle R_{\perp}^2 \rangle$ first shrinks and when $D < D_c$ the size starts to grow.

D_c follows the same 3d Flory-scaling form as the size of an excluded volume polymer freely floating in 3d. Thus the position of this minimum scaled by the bulk polymer size (end-to-end distance or radius of gyration) $D_c/L^{3/5}$ should be independent of polymer contour-length L . The MC simulation results shown in Fig.1 of Ref.[19] corroborate this fact.

IV. SIMULATIONS

In the previous two sections we demonstrated scaling arguments and a mean field theory to obtain estimates for the size and shape of confined excluded volume polymers. To validate our mean field picture, we present the results of a full numerical simulation for such a system.

A. Method

We perform molecular dynamics simulations of a self avoiding bead-spring chain trapped between two soft-walls in presence of a Langevin heat bath. All the beads interact via the fully repulsive part of Lennard-Jones potential $V_{LJ}^{rep}(r) = 4\epsilon [(\sigma/r)^{12} - (\sigma/r)^6 + 1/4]$, with a cut-off distance set to $r_c = 2^{1/6}\sigma$ so that $V_{LJ}^{rep}(r \geq r_c) = 0$. ϵ is the strength and σ is the range of the interaction. The bond between two neighboring beads are modeled by a *shifted* harmonic potential $V_{sp}(r) = (A/2)(r - \sigma)^2$ with spring constant $A = 100\epsilon/\sigma^2$ such that the equilibrium bond-length, in absence of any other forces, is σ . r denotes the center-to-center distance between a pair of beads. We assume that the polymer is confined within two parallel walls placed at $z = -D/2, D/2$. The repulsive potential due to the walls is assumed to be the integrated and shifted Lennard-Jones potential $V_{wall}(\delta z) = \epsilon [(\sigma/\delta z)^{10} - (\sigma/\delta z)^4 + g]$ with $g = (5/2 - 1)(2/5)^{5/3}$ and a cut-off distance $z_c = (5/2)^{1/6}\sigma$, so that $V_{wall}(|\delta z| \geq z_c) = 0$. Here δz is the z -separation of a bead from any one of the walls (top or bottom). ϵ and σ set the energy and length scales, respectively. We integrate Langevin equations using the velocity-Verlet algorithm[29] with a time-step $\delta t = 0.01\tau$ where $\tau = \sigma\sqrt{m}/\epsilon$ is the characteristic time scale. We set the mass of each bead $m = 1$ and isotropic friction coefficient $\gamma = 1/\tau$. The Langevin thermostat[30] is used to keep the system at a constant temperature $T = 1.0\epsilon/k_B$.

B. Results

The quantity we are interested in is the equilibrium size and shape of the polymer. In the model we simulate,

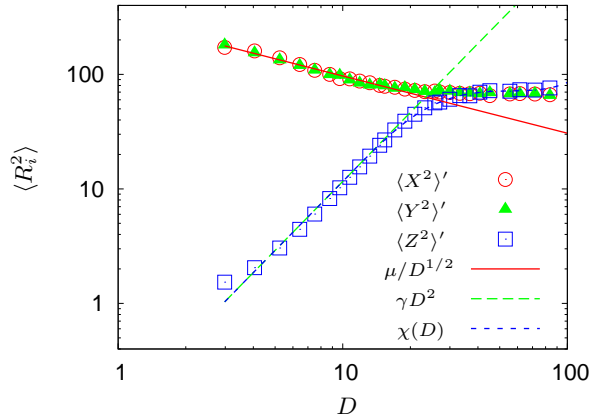


FIG. 2: (Color online) Components of mean squared end-to-end distance $\langle R_i^2 \rangle$ as a function of plate-separation D . All lengths are expressed in units of σ . We have plotted the components $\langle X^2 \rangle' = \langle X^2 \rangle - \lambda_{\parallel}$, $\langle Y^2 \rangle' = \langle Y^2 \rangle - \lambda_{\parallel}$, and $\langle Z^2 \rangle' = \langle Z^2 \rangle + \lambda_{\perp}$ where λ_{\parallel} and λ_{\perp} are offset polymer sizes (see main text). With decreasing D , $\langle X^2 \rangle$ and $\langle Y^2 \rangle$ increases in the same manner while $\langle Z^2 \rangle$ decreases. All the components obey de Gennes scaling, up to the leading order: $\langle X^2 \rangle' = \langle Y^2 \rangle' = \mu/D^{1/2}$, and $\langle Z^2 \rangle' = \gamma D^2$ where $\mu = 306$ and $\gamma = 0.12$. The fitted values of offsets are $\lambda_{\parallel} = 12.8 \pm 4.2$ and $\lambda_{\perp} = 1.4$. At larger D , $\langle Z^2 \rangle'$ shifts from the scaling form (Eq.17) as $\chi(D) = \gamma D^2 - c_1 D^2 \exp(-c_2/D^2 + c_3/D^{1/2})$ where $c_1 = 0.1$, $c_2 = 970$ and $c_3 = 2.06 \pm 0.36$. The fitting error in all the parameters is less than 5%, unless specified otherwise.

the polymer is made of $i = 1, \dots, N$ beads with a mean contour length $L = (N - 1)$ in units of σ . We follow the mean squared end-to-end distance in the confining z -direction $\langle Z^2 \rangle = \langle (z_N - z_1)^2 \rangle$ as well as in the unconfined xy -plane $\langle X^2 \rangle = \langle (x_N - x_1)^2 \rangle$, $\langle Y^2 \rangle = \langle (y_N - y_1)^2 \rangle$. The time evolution of these quantities allows us to identify the equilibration of the system. In order to test the validity of our simulation scheme, in a separate simulation of the bulk-system (using periodic boundary conditions in all three directions) we measured $\langle R_{\text{bulk}}^2 \rangle = \langle X^2 \rangle + \langle Y^2 \rangle + \langle Z^2 \rangle$ as a function of polymer contour length $L = 8, 16, 32, 64, 128, 256$ to obtain Flory scaling $\langle R_{\text{bulk}}^2 \rangle \sim L^{6/5}$ (data not shown).

For the simulations of confined system we used an $N = 64$ bead polymer. The simulations were equilibrated for $10^6 \tau$ before collecting data over further $3 \times 10^8 \tau$. We used periodic boundary conditions in x and y directions with the lateral extent of the simulation box in these directions $W = 2L$. In Fig.2 we have plotted the three components of mean squared end-to-end distance $\langle X^2 \rangle' = \langle X^2 \rangle - \lambda_{\parallel}$, $\langle Y^2 \rangle' = \langle Y^2 \rangle - \lambda_{\parallel}$, and $\langle Z^2 \rangle' = \langle Z^2 \rangle + \lambda_{\perp}$ where λ_{\parallel} and λ_{\perp} are offset polymer sizes which comes about for reasons discussed in the following.

The mean squared end-to-end distance in the confining direction $\langle Z^2 \rangle'$ shrinks with increasing degree of confinement (decreasing D) as γD^2 (Fig.2). Apart from an additive offset λ_{\perp} , this is consistent with the leading order

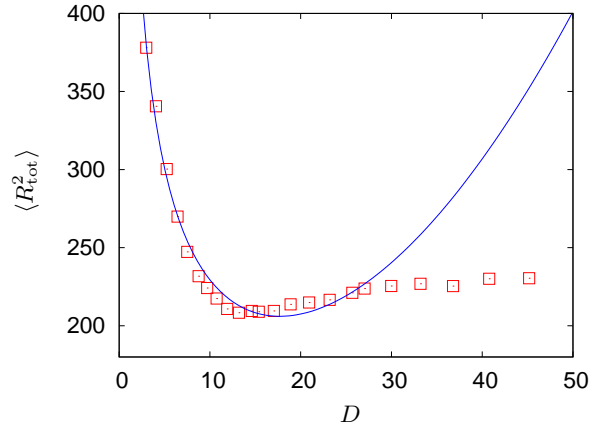


FIG. 3: (Color online) Mean squared end-to-end distance $\langle R_{\text{tot}}^2 \rangle = \langle X^2 \rangle + \langle Y^2 \rangle + \langle Z^2 \rangle$ as a function of plate-separation D . The line is a plot of $2(\mu/D^{1/2} + \lambda_{\parallel}) + (\gamma D^2 - \lambda_{\perp})$ where we used the same values of μ , γ , λ_{\parallel} and λ_{\perp} as in Fig.2.

behavior predicted by our MFT [Eq. (17)] and de Gennes scaling. Due to a finite non-zero range of repulsion z_c coming from the soft-wall confinement (not incorporated in the MFT as in the MFT we assumed hard wall confinement for simplicity), simulated $\langle Z^2 \rangle$ gets suppressed by an extra amount λ_{\perp} . This indicates that λ_{\perp} should be a function of z_c which vanishes as $z_c \rightarrow 0$ (hard wall limit). The fitting procedure in Fig.2 gives $\lambda_{\perp} = 1.4 \pm 0.06$ which is numerically indistinguishable from $z_c^2 = 1.36$. At larger D , we find a saturation of $\langle Z^2 \rangle$ that obeys the functional form (Fig.2)

$$\chi(D) = \gamma D^2 - c_1 D^2 \exp(-c_2/D^2 + c_3/D^{1/2}).$$

Notice that this form of $\chi(D)$ is obtained from the expression of $\langle R_{\perp}^2 \rangle$ obtained from Eqs. (17) and (15).

Fig.2 clearly shows that with increasing degree of confinement, the components of mean squared end-to-end separation in the unconfined directions expands $\langle X^2 \rangle' = \langle Y^2 \rangle' = \mu/D^{1/2}$. Leaving out the offset value λ_{\parallel} , this obeys de Gennes scaling. Note that an offset like λ_{\parallel} was expected from our MFT [see the first line of Eq. (18)]. Further, the excess compression of $\langle Z^2 \rangle$ by λ_{\perp} requires an extra bit of expansion in the parallel components. λ_{\parallel} contains this contribution too. At large enough plate-separations $\langle X^2 \rangle$, $\langle Y^2 \rangle$ saturate to their bulk value.

The total mean squared end-to-end distance of the confined-polymer $\langle R_{\text{tot}}^2 \rangle = \langle X^2 \rangle + \langle Y^2 \rangle + \langle Z^2 \rangle$ shows a non-monotonic dependence on D (Fig.3). $\langle R_{\text{tot}}^2 \rangle$, starting from its bulk value at large D , first reduces to reach a minimum and then expands as we reduce the plate separation. The initial decrease in size is mainly governed by the shrinkage in $\langle Z^2 \rangle$. At small D values, the large increase of the polymer-size in the unconfined directions $\langle X^2 \rangle$ and $\langle Y^2 \rangle$ takes over. The cross-over between these two different behaviors takes place at the minimum of $\langle R_{\text{tot}}^2 \rangle$, a feature predicted by the MFT [Eq. (48)] as well as by de Gennes scaling (Sec.II). Fig.3 shows that the

scaling forms added with the offset parameters in the three components of the mean squared end-to-end distance does capture the non-monotonicity as well as the approximate position of the minimum in $\langle R_{\text{tot}}^2 \rangle$.

V. DISCUSSION AND OUTLOOK

In this paper we have presented a mean field approach to calculate the mean squared end-to-end distance of a self-avoiding polymer confined within a parallel-plate geometry. The method allowed us to calculate all the components of this quantity separately as a function of plate-separation. Up to the leading order calculation, we recovered Flory scaling in the limit of large plate separations (bulk limit), and de Gennes scaling in the limit of small plate separations. The next to leading order correction allows a smooth transition from de Gennes regime towards Flory regime. We believe that higher order perturbation calculations using our MFT framework will further bridge the gap between the two regimes. We noted that the non-monotonicity of the overall polymer size as a function of the increased degree of confinement, as clearly captured by our MFT, was already inherent to de Gennes scaling. The numerical results from Langevin dynamics simulations showed good agreement with our MFT predictions.

It is, however, hard to make quantitative comparisons between the theoretical calculations and the simulations for quantities like actual prefactors of scaling laws. There are two reasons behind this. First, these non-universal quantities depend on the detailed nature and strength of the interactions. Secondly, as was already discussed in Ref.[26], the effective values of the prefactors in the scaling forms depend on up to which order the perturbative calculations are performed in the MFT.

Before we end the discussion, we would like to emphasize the simple fact that with decreasing plate-separations, the polymer size in the confining direction can only shrink, while it expands in the other unconfined directions. In a recent experiment on DNA confined between two parallel plates [10], the average radius of gyration was measured from the configurations projected onto a plane parallel to the confining glass plates. Ref. [10] showed that with reducing plate-separation D , this *projected* radius of gyration first shrank, before expanding in accordance with de Gennes scaling $D^{-1/4}$. Similar non-monotonic features were also reported in Ref. [11]. This behavior should not be confused with the non-monotonicity in $\langle R_{\text{tot}}^2 \rangle$ (Fig.3) and is clearly not in agreement with our assertion mentioned above. Ref. [11] speculated that this non-monotonicity may be due to attractive interaction with the confining walls, as the detailed nature of polymer-wall interaction is both hard to control and to determine in experiments. It should be noted, however, that the non-monotonicity in the radius of gyration calculated from the full 3d configurations of a confined self-avoiding polymer, as observed in

our Langevin dynamics simulations (data not shown) and previous Monte-Carlo simulations [19], has a different origin. It is purely an entropic effect caused by the hard confinement and, as we have shown in Sec. II, is already to be expected on the basis of de Gennes scaling. Using our Langevin dynamics simulations, we have also evaluated the radius of gyration of the excluded volume polymer confined between two parallel plates from configurations projected onto a plane parallel to the plates, exactly in the same manner as described in Ref. [10]. These simulations showed a clear monotonic increase as $D^{-1/4}$ with reducing D (data not shown). This is in contrast to the observed behavior in Refs. [10, 11], and in agreement with our assertion that polymer size in the unconfined directions can only monotonically grow with increasing degree of confinement.

Finally, the MFT approach used in this paper can be easily extended to other confining geometries, e.g., cubic or cylindrical pores. The cylindrical confinement is a natural choice for the study of bacterial chromosomes [5]. Within a biological cell, binding of proteins on DNA may enhance (or reduce) the effective persistence length of DNA. Thus it would be interesting to examine the effect of varying bending stiffness on confined polymers. A similar MFT method may potentially also be used to describe tethered polymers. For this case one may need to self-consistently determine the step-size of the effective Gaussian polymer as a function of distance from the tethered end. Thus, this mean field approach has the potential to provide analytical access to many situations of biological relevance.

Acknowledgments

This work is part of the research program of the Stichting voor Fundamenteel Onderzoek der Materie (FOM), which is supported by the Nederlandse organisatie voor Wetenschappelijk Onderzoek (NWO). DC is funded by project 07DNAA02 in the FOM-program #103 “DNA in action: Physics of the genome”. We thank C. Dekker for discussions on Ref. [10], and Nils Becker for a critical reading of the manuscript.

Appendix A: Calculating Green’s function

A separation of variable $G_0 = f(L)\psi(\mathbf{r}_{\parallel})\phi(z)$ in Eq. (20) leads to,

$$\frac{1}{f} \frac{df}{dL} = \frac{l_{\parallel}}{6} \frac{1}{\psi} \nabla_{\parallel}^2 \psi + \frac{l_{\perp}}{6} \frac{1}{\phi} \frac{d^2 \phi}{dz^2} \equiv -E \quad (\text{A1})$$

where E is an arbitrary constant. Further, let us assume,

$$\left(\frac{d^2}{dz^2} + k_z^2 \right) \phi(z) = 0 \quad (\text{A2})$$

$$\left(\nabla_{\parallel}^2 + \mathbf{k}_{\parallel}^2 \right) \psi(\mathbf{r}_{\parallel}) = 0. \quad (\text{A3})$$

The Dirichlet boundary condition $G_0(z = 0, D) = 0$ requires the solution, $\phi_n(z) = \sqrt{2/D} \sin(k_z^n z) \sqrt{2/D} \sin(k_z^n z')$ with $k_z^n = (n\pi/D)$, n being a positive integer. The solution in the x and y directions gives $\psi(\mathbf{r}_{\parallel}) = \exp(i\mathbf{k}_{\parallel} \cdot \mathbf{r}_{\parallel})$ with a continuum of \mathbf{k}_{\parallel} modes in presence of an open boundary condition. Eq. (A1) leads to the identity,

$$E = \frac{l_{\parallel}}{6} \mathbf{k}_{\parallel}^2 + \frac{l_{\perp}}{6} \left(\frac{n\pi}{D} \right)^2. \quad (\text{A4})$$

Thus the solution of the differential equation Eq. (20) has the form $\exp(-EL) \exp(i\mathbf{k}_{\parallel} \cdot \mathbf{r}_{\parallel}) \sin(k_z^n z) \sin(k_z^n z')$. The general solution is obtained by summing (integrating) over all possible modes n (\mathbf{k}_{\parallel}),

$$\begin{aligned} G_0 &= \frac{2}{D} \int \frac{d\mathbf{k}_{\parallel}}{(2\pi)^2} \sum_{n=1}^{\infty} e^{-(l_{\parallel}/6)\mathbf{k}_{\parallel}^2 L - (l_{\perp}/6)(n\pi/D)^2 L} e^{i\mathbf{k}_{\parallel} \cdot (\mathbf{r}_{\parallel} - \mathbf{r}'_{\parallel})} \sin\left(\frac{n\pi}{D} z\right) \sin\left(\frac{n\pi}{D} z'\right) \\ &= \frac{3}{2\pi l_{\parallel} L} e^{-3(\mathbf{r}_{\parallel} - \mathbf{r}'_{\parallel})^2 / 2l_{\parallel} L} \times \frac{2}{D} \sum_{n=1}^{\infty} e^{-(l_{\perp}/6)(n\pi/D)^2 L} \sin\left(\frac{n\pi}{D} z\right) \sin\left(\frac{n\pi}{D} z'\right) \equiv G_{\parallel} \times G_{\perp}. \end{aligned} \quad (\text{A5})$$

Appendix B: Contributions from excluded volume interactions

In this appendix we calculate δ_{\parallel}^b and δ_{\perp}^b .

The first order contributions due to the excluded volume term in the Hamiltonian are of the form

$$\begin{aligned} \langle A(\mathbf{r}(0), \mathbf{r}(L)) \beta \Delta \mathcal{H}_b \rangle_0 &= \\ \frac{1}{Z} \frac{1}{2} b \int d\mathbf{r}(0) \int d\mathbf{r}(L) A(\mathbf{r}(0), \mathbf{r}(L)) \int_0^L ds \int_0^L ds' & \\ \int_{\mathbf{r}(0)}^{\mathbf{r}(L)} \mathcal{D}[\mathbf{r}(s)] \delta(\mathbf{r}(s) - \mathbf{r}(s')) \exp\{-\beta \mathcal{H}_0[\mathbf{r}(s)]\} & \\ \equiv \frac{1}{Z} \frac{1}{2} b \int d\mathbf{r}(0) \int d\mathbf{r}(L) A(\mathbf{r}(0), \mathbf{r}(L)) & \\ \int_0^L ds \int_0^L ds' E(s, s' | \mathbf{r}(0), \mathbf{r}(L)), & \end{aligned}$$

where the integration over end-points are performed for all possible $\mathbf{r}(0)$ and $\mathbf{r}(L)$. We consider the evaluation of the kernel $E(s, s' | \mathbf{r}(0), \mathbf{r}(L))$ of the inner integration, assuming for the moment that $s > s'$. The Chapman-Kolmogorov property

$$G(\mathbf{r}, L | \mathbf{r}', 0) = \int d\mathbf{r}'' G(\mathbf{r}, L | \mathbf{r}'', L-s) G(\mathbf{r}'', s | \mathbf{r}', 0) \quad (\text{B1})$$

then allows us to write

$$\begin{aligned} E(s, s' | \mathbf{r}(\mathbf{0}), \mathbf{r}(\mathbf{L})) &= \int d\mathbf{r}' \mathbf{G}_0(\mathbf{r}(\mathbf{L}), \mathbf{L} | \mathbf{r}', s) \\ &G_0(\mathbf{r}', s | \mathbf{r}', s') \mathbf{G}_0(\mathbf{r}', s' | \mathbf{r}(\mathbf{0}), \mathbf{0}). \end{aligned} \quad (\text{B2})$$

We also use the fact that since the Green's function factorizes as $G_0 = G_{\parallel} G_{\perp}$, the separation of variable works

for $E = E_{\parallel}(s, s' | \mathbf{r}_{\parallel}(0), \mathbf{r}_{\parallel}(L)) \times E_{\perp}(s, s' | r_{\perp}(0), r_{\perp}(L))$ as well.

As the longitudinal part is unaffected by the constraints, it is the simplest case. Indeed, as

$$G_{\parallel}(\mathbf{r}', s | \mathbf{r}', s') = \frac{3}{2\pi l_{\parallel} (s - s')} \quad (\text{B3})$$

does not depend on the intermediate position \mathbf{r}'_{\parallel} we immediately find that

$$\begin{aligned} E_{\parallel}(s, s' | \mathbf{r}_{\parallel}(0), \mathbf{r}_{\parallel}(L)) &= \\ = \frac{3}{2\pi l_{\parallel} (s - s')} G_{\parallel}(\mathbf{r}_{\parallel}(L), L - (s - s') | \mathbf{r}_{\parallel}(0), 0) \end{aligned} \quad (\text{B4})$$

A similar simplification does not hold for the transverse component as

$$G_{\perp}(r'_{\perp}, s | r'_{\perp}, s') = \frac{2}{D} \sum_{n=1}^{\infty} \sin^2\left(\frac{n\pi}{D} r'_{\perp}\right) e^{-\kappa n^2 (s - s')} \quad (\text{B5})$$

(with $\kappa = (l_{\perp}/6)(\pi/D)^2$) does depend on r'_{\perp} . We therefore find that

$$\begin{aligned} E_{\perp}(s, s' | r_{\perp}(0), r_{\perp}(L)) &= \\ = \frac{1}{D^2} \sum_{n_L, n', n_0=1}^{\infty} e^{-\kappa n_L^2} e^{-\kappa s(n'^2 - n_L^2)} e^{-\kappa s'(n_0^2 - n'^2)} & \\ \times [2\delta_{n_0, n_L} + \delta_{n', (n_0 + n_L)/2} - \delta_{n', (n_0 - n_L)/2} - \delta_{n', (n_L - n_0)/2}] & \\ \times \sin\left(\frac{n_L \pi}{D} r_{\perp}(L)\right) \sin\left(\frac{n_0 \pi}{D} r_{\perp}(0)\right), \end{aligned} \quad (\text{B6})$$

Again, we can write

$$\langle R_{\parallel}^2 \beta \Delta \mathcal{H}_b \rangle_0 = Z^{-1} \frac{1}{2} b \int_0^L ds \int_0^L ds' \int d\mathbf{r}(\mathbf{0}) \int d\mathbf{r}(\mathbf{L})$$

$$\begin{aligned}
& [\mathbf{r}_{\parallel}(L) - \mathbf{r}_{\parallel}(0)]^2 E(s, s' | \mathbf{r}(\mathbf{0}), \mathbf{r}(\mathbf{L})) \\
&= Z^{-1} \frac{1}{2} b \int_0^L ds \int_0^L ds' \\
& \left[\int d\mathbf{r}_{\parallel}(0) \int d\mathbf{r}_{\parallel}(L) [\mathbf{r}_{\parallel}(L) - \mathbf{r}_{\parallel}(0)]^2 E_{\parallel} \right] \\
& \left[\int dr_{\perp}(0) \int dr_{\perp}(L) E_{\perp} \right] \\
&\equiv Z^{-1} \frac{1}{2} b \int_0^L ds \int_0^L ds' I_{\parallel}^2(s, s') I_{\perp}^0(s, s').
\end{aligned} \tag{B7}$$

Similarly,

$$\langle R_{\perp}^2 \beta \Delta \mathcal{H}_b \rangle_0 = Z^{-1} \frac{1}{2} b \int_0^L ds \int_0^L ds' I_{\parallel}^0(s, s') I_{\perp}^2(s, s'). \tag{B8}$$

$$\langle \beta \Delta \mathcal{H}_b \rangle_0 = Z^{-1} \frac{1}{2} b \int_0^L ds \int_0^L ds' I_{\parallel}^0(s, s') I_{\perp}^0(s, s'). \tag{B9}$$

In the above, we used the definitions

$$I_{\parallel}^0(s, s') = \int d\mathbf{r}_{\parallel}(0) \int d\mathbf{r}_{\parallel}(L) E_{\parallel}(s, s' | \mathbf{r}_{\parallel}(0), \mathbf{r}_{\parallel}(L)) \tag{B10}$$

$$\begin{aligned}
I_{\parallel}^2(s, s') &= \int d\mathbf{r}_{\parallel}(0) \int d\mathbf{r}_{\parallel}(L) E_{\parallel}(s, s' | \mathbf{r}_{\parallel}(0), \mathbf{r}_{\parallel}(L)) \\
& \times (\mathbf{r}_{\parallel}(L) - \mathbf{r}_{\parallel}(0))^2
\end{aligned} \tag{B11}$$

$$I_{\perp}^0(s, s') = \int dr_{\perp}(0) \int dr_{\perp}(L) E_{\perp}(s, s' | r_{\perp}(0), r_{\perp}(L)) \tag{B12}$$

$$\begin{aligned}
I_{\perp}^2(s, s') &= \int dr_{\perp}(0) \int dr_{\perp}(L) E_{\perp}(s, s' | r_{\perp}(0), r_{\perp}(L)) \\
& \times (r_{\perp}(L) - r_{\perp}(0))^2.
\end{aligned} \tag{B13}$$

We can now evaluate the integrals over the end points. The longitudinal ones are easier to compute,

$$\begin{aligned}
I_{\parallel}^0(s, s') &= W^2 \frac{3}{2\pi l_{\parallel}(s-s')} \\
I_{\parallel}^2(s, s') &= W^2 \frac{3}{2\pi l_{\parallel}(s-s')} \times \frac{2}{3} l_{\parallel}(L - (s-s')).
\end{aligned} \tag{B14}$$

The only $r_{\perp}(0)$ and $r_{\perp}(L)$ dependent term present in $E_{\perp}(s, s' | r_{\perp}(0), r_{\perp}(L))$ is $q(r_{\perp}(L), r_{\perp}(0)) = \sin(n_L \pi r_{\perp}(L)/D) \times \sin(n_0 \pi r_{\perp}(0)/D)$. To evaluate the integration in $I_{\perp}^0(s, s')$ we use the identity

$$\int_0^D dr_{\perp} \sin\left(\frac{n\pi}{D} r_{\perp}\right) = \frac{D}{n\pi} [1 - (-1)^n]. \tag{B15}$$

Thus,

$$\begin{aligned}
I_{\perp}^0(s, s') &= \sum_{n_L, n', n_0=1}^{\infty} e^{-\kappa n_L n_L^2} e^{-\kappa s(n'^2 - n_L^2)} e^{-\kappa s'(n_0^2 - n'^2)} \\
& \times [2\delta_{n_0, n_L} + \delta_{n', (n_0+n_L)/2} \\
& - \delta_{n', (n_0-n_L)/2} - \delta_{n', (n_L-n_0)/2}] J_0(n_L, n_0)
\end{aligned} \tag{B16}$$

where

$$J_0(n_L, n_0) = \frac{1}{n_0 n_L \pi^2} [1 - (-1)^{n_L}] [1 - (-1)^{n_0}]. \tag{B17}$$

To calculate $I_{\perp}^2(s, s')$ one requires to use the integration of sine function with powers, such as, $\int_0^D dr \sin(n\pi r/D)$, $\int_0^D dr r \sin(n\pi r/D)$, and $\int_0^D dr r^2 \sin(n\pi r/D)$. This gives us,

$$\begin{aligned}
I_{\perp}^2(s, s') &= D^2 \sum_{n_L, n', n_0=1}^{\infty} e^{-\kappa n_L n_L^2} e^{-\kappa s(n'^2 - n_L^2)} e^{-\kappa s'(n_0^2 - n'^2)} \\
& \times [2\delta_{n_0, n_L} + \delta_{n', (n_0+n_L)/2} \\
& - \delta_{n', (n_0-n_L)/2} - \delta_{n', (n_L-n_0)/2}] \\
& \times J(n_L, n_0),
\end{aligned} \tag{B18}$$

where,

$$\begin{aligned}
J(n_L, n_0) &= -\frac{1}{n_L^3 n_0 \pi^4} [(-1)^{n_L} n_L^2 \pi^2 + 2(1 - (-1)^{n_L})] \\
& \times [1 - (-1)^{n_0}] - \frac{2}{n_L n_0 \pi^2} (-1)^{n_0} (-1)^{n_L} \\
& - \frac{1}{n_L n_0^3 \pi^4} [(-1)^{n_0} n_0^2 \pi^2 + 2(1 - (-1)^{n_0})] \\
& \times [1 - (-1)^{n_L}].
\end{aligned} \tag{B19}$$

We used $s > s'$ in the above. Now, using the identity

$$\frac{1}{2} \int_0^L ds \int_0^L ds' = \int_0^L ds' \int_{s'}^L ds \tag{B20}$$

we have

$$\delta_{\parallel}^b = Z^{-1} b \int_0^L ds' \int_{s'}^L ds I_{\perp}^0(s, s') [I_{\parallel}^2(s, s') - \langle R_{\parallel}^2 \rangle_0 I_{\parallel}^0(s, s')] \tag{B21}$$

$$\delta_{\perp}^b = Z^{-1} b \int_0^L ds' \int_{s'}^L ds I_{\parallel}^0(s, s') [I_{\perp}^2(s, s') - \langle R_{\perp}^2 \rangle_0 I_{\perp}^0(s, s')]. \tag{B22}$$

We now have all the ingredients to calculate the perturbation corrections.

1. Parallel Component δ_{\parallel}^b

We have,

$$\begin{aligned} & [I_{\parallel}^2(s, s') - \langle R_{\parallel}^2 \rangle_0 I_{\parallel}^0(s, s')] \\ &= \frac{3W^2}{2\pi l_{\parallel}(s-s')} \times \left(\frac{2}{3} l_{\parallel}(L - (s-s')) - \frac{2}{3} l_{\parallel}L \right) = -\frac{W^2}{\pi}. \end{aligned} \quad (\text{B23})$$

Thus in evaluating the integral in δ_{\parallel}^b (Eq. B21), we need to do the following integration,

$$M = e^{-\kappa L n_L^2} \int_0^L ds' \int_{s'}^L ds e^{-\kappa s(n'^2 - n_L^2)} e^{-\kappa s'(n_0^2 - n'^2)} \quad (\text{B24})$$

where the only function of (s, s') in the integrand comes from $I_{\perp}^0(s, s')$.

Thus, we obtain,

$$\begin{aligned} \delta_{\parallel}^b &= -\frac{b}{Z} W^2 \frac{1}{\pi} \sum_{n_L, n', n_0=1}^{\infty} M(n_L, n', n_0; \kappa) \\ &\times [2\delta_{n_0, n_L} + \delta_{n', (n_0+nL)/2} \\ &\quad - \delta_{n', (n_0-nL)/2} - \delta_{n', (nL-n_0)/2}] J_0(n_L, n_0), \end{aligned}$$

i.e., Eq. 36.

2. Perpendicular Component δ_{\perp}^b

The only function of (s, s') in Eq. B22 is $\exp[-\kappa s(n'^2 - n_L^2)] \exp[-\kappa s'(n_0^2 - n'^2)]$ due to the function $[I_{\perp}^2(s, s') - \langle R_{\perp}^2 \rangle_0 I_{\perp}^0(s, s')]$ and $1/(s-s')$ due to $I_{\parallel}^0(s, s')$. Thus we have to evaluate the integration,

$$K = e^{-\kappa L n_L^2} \int_0^L ds' \int_{s'}^L ds \frac{e^{-\kappa s(n'^2 - n_L^2)} e^{-\kappa s'(n_0^2 - n'^2)}}{(s-s')}. \quad (\text{B25})$$

The term by term calculation of this quantity for each (n_0, n', n_L) encounters a pole at $s = s'$. To avoid the pole, the integration to evaluate Eq. (B25) can be rewritten as,

$$\begin{aligned} K(n_L, n', n_0; \kappa) &= e^{-\kappa L n_L^2} \lim_{a \rightarrow 0} \int_0^L ds' \int_{s'}^L ds \\ &\quad \left[\frac{e^{-\kappa s(n'^2 - n_L^2)} e^{-\kappa s'(n_0^2 - n'^2)}}{(s-s') + a} \right]. \end{aligned} \quad (\text{B26})$$

Note that this is equivalent to replacing the delta-function overlap-interaction by its Gaussian representation but keeping a non-zero variance a^2 . Thus we obtain the expression (Eq. 39),

$$\begin{aligned} \delta_{\perp}^b &= \frac{b}{Z} W^2 \frac{3}{2\pi l_{\parallel}} \sum_{n_L, n', n_0=1}^{\infty} D^2 K(n_L, n', n_0; \kappa) \\ &\times [2\delta_{n_0, n_L} + \delta_{n', (n_0+nL)/2} \end{aligned}$$

$$\begin{aligned} & - \delta_{n', (n_0-nL)/2} - \delta_{n', (nL-n_0)/2}] \\ &\times \left[J(n_L, n_0) - \frac{\langle R_{\perp}^2 \rangle_0}{D^2} J_0(n_L, n_0) \right]. \end{aligned}$$

Appendix C: Bulk limit of $D \rightarrow \infty$

In this appendix we calculate δ_{\parallel}^b , δ_{\perp}^b and δ_{\perp}^{\perp} in the bulk limit of $D \rightarrow \infty$.

It is clear that, since in this limit G_{\perp} itself is independent of D , δ_{\parallel}^b and δ_{\perp}^b are also independent of D . Using the continuum approach at $D \rightarrow \infty$,

$$\begin{aligned} E_{\perp} &= \sqrt{\frac{3}{2\pi l_{\perp}(s-s')}} G_{\perp}(z(L), L - (s-s') | z(0), 0) \\ &= \sqrt{\frac{3}{2\pi l_{\perp}(s-s')}} \times \sqrt{\frac{3}{2\pi l_{\perp}(L - (s-s'))}} \\ &\times \exp\left[-\frac{3}{2} \frac{(z(L) - z(0))^2}{l_{\perp}(L - (s-s'))}\right]. \end{aligned} \quad (\text{C1})$$

Then using Eq. B12 we get

$$\begin{aligned} I_{\perp}^0(s, s') &= \int dz(0) \int dz(L) E_{\perp}(s, s' | r_{\perp}(0), r_{\perp}(L)) \\ &= D \sqrt{\frac{3}{2\pi l_{\perp}(s-s')}}. \end{aligned} \quad (\text{C2})$$

Remember that, now, the orthogonal component of partition function has also got redefined to $Z_{\perp} = D$. Then using Eq. B21,

$$\begin{aligned} \delta_{\parallel}^b &= Z^{-1} b \int_0^L ds' \int_{s'}^L ds I_{\perp}^0(s, s') [I_{\parallel}^2(s, s') - \langle R_{\parallel}^2 \rangle_0 I_{\parallel}^0(s, s')] \\ &= (W^2 D)^{-1} b (-W^2/\pi) \\ &\times D \sqrt{\frac{3}{2\pi l_{\perp}}} \int_0^L ds' \int_{s'}^L ds \sqrt{\frac{1}{(s-s')}} \\ &= -\frac{b}{\pi} \times \sqrt{\frac{3}{2\pi l_{\perp}}} \times \frac{4}{3} L^{3/2}; \end{aligned} \quad (\text{C3})$$

where we also used Eqs. B14 and 27. Using Eq. B13 we find

$$\begin{aligned} I_{\perp}^2(s, s') &= \int_{-\infty}^{\infty} dz(0) \int_{-\infty}^{\infty} dz(L) \sqrt{\frac{3}{2\pi l_{\perp}(s-s')}} \\ &\times \sqrt{\frac{3}{2\pi l_{\perp}(L - (s-s'))}} e^{-\frac{3(z(L) - z(0))^2}{2l_{\perp}(L - (s-s'))}} \\ &= \sqrt{\frac{3}{2\pi l_{\perp}(s-s')}} D \frac{l_{\perp}(L - (s-s'))}{3} \end{aligned} \quad (\text{C4})$$

and using Eq. 28 we get

$$\langle R_{\perp}^2 \rangle_0 = \frac{\int_{-\infty}^{\infty} dz \int_{-\infty}^{\infty} dz' (z-z')^2 e^{-\frac{3(z(L) - z(0))^2}{2l_{\perp}L}}}{\int_{-\infty}^{\infty} dz \int_{-\infty}^{\infty} dz' e^{-\frac{3(z(L) - z(0))^2}{2l_{\perp}L}}}$$

$$= \frac{l_{\perp} L}{3}. \quad (\text{C5})$$

Therefore,

$$I_{\perp}^2(s, s') - \langle R_{\perp}^2 \rangle_0 I_{\perp}^0(s, s') = -D \frac{l_{\perp}}{6\pi} (s - s')^{1/2}, \quad (\text{C6})$$

and

$$\begin{aligned} & I_{\parallel}^0(s, s') [I_{\perp}^2(s, s') - \langle R_{\perp}^2 \rangle_0 I_{\perp}^0(s, s')] \\ &= -W^2 \frac{3}{2\pi l_{\parallel} (s - s')} D \sqrt{\frac{l_{\perp}}{6\pi}} (s - s')^{1/2} \\ & - W^2 \frac{D l_{\perp}^{1/2}}{l_{\parallel}} (s - s')^{-1/2}. \end{aligned} \quad (\text{C7})$$

Since in this limit $Z = W^2 D$, using Eq. B22 we find,

$$\begin{aligned} \delta_{\perp}^b &= Z^{-1} b \int_0^L ds' \int_{s'}^L ds I_{\parallel}^0(s, s') \\ & \times [I_{\perp}^2(s, s') - \langle R_{\perp}^2 \rangle_0 I_{\perp}^0(s, s')] \\ & \simeq -\frac{b l_{\perp}^{1/2}}{l_{\parallel}} L^{3/2} \end{aligned} \quad (\text{C8})$$

Similarly, using Eq. C5 in Eq. 34, we obtain

$$\delta_{\perp}^{\perp} = -\frac{3}{2} \left(\frac{1}{l} - \frac{1}{l_{\perp}} \right) \frac{\partial}{\partial \alpha_{\perp}} \langle R_{\perp}^2 \rangle_0 = \frac{1}{3} \left(\frac{1}{l} - \frac{1}{l_{\perp}} \right) L l_{\perp}^2. \quad (\text{C9})$$

Appendix D: 2d limit of confined system

In pure 2d, the perturbative contribution due to the inter-segment interactions takes the form,

$$\delta_{2d}^b = Z_{2d}^{-1} b_0 \int_0^L ds' \int_{s'}^L ds [I_{\parallel}^2(s, s') - \langle R_{\parallel}^2 \rangle_0 I_{\parallel}^0(s, s')]$$

where $Z_{2d} = W^2$. Thus,

$$\delta_{2d}^b = -\frac{b_0}{2\pi} L^2$$

where b_0 plays the role of interaction strength. Thus, $\delta_{\parallel} = \delta_{\parallel}^{\parallel} + \delta_{\parallel}^b = 0$ implies

$$\begin{aligned} \frac{L l_{2d}^2}{l} &\sim \frac{b_0}{2\pi} L^2 \\ \text{or, } l_{2d} &\sim (b_0 l)^{1/2} L^{1/2} \end{aligned}$$

which leads to the scaling form,

$$\langle R_{2d}^2 \rangle \sim L l_{2d} \sim (b_0 l)^{1/2} L^{3/2}. \quad (\text{D1})$$

We expect that the polymer would behave like a pure 2d polymer in the limit of extremely small plate-separation D . This limit is achieved when $\langle R_{\parallel}^2 \rangle = \langle R_{2d}^2 \rangle$. We have seen that the strength of the interaction b in 3d has the dimension of length, whereas the same strength b_0 is dimension-less in 2d. This shows that the only intrinsic microscopic length scale in the system is segment-length l . Thus we need to express $b = b_0 l$ to search for the pure 2d limit of confined systems. With this substitution,

$$\langle R_{\parallel}^2 \rangle \sim (b_0 l)^{1/2} L^{3/2} \left(\frac{l}{D} \right)^{1/2}. \quad (\text{D2})$$

Therefore, $\langle R_{\parallel}^2 \rangle$ equates $\langle R_{2d}^2 \rangle$ when $D \sim l$, i.e., when the plate-separation D becomes as small as the polymer segment-length l .

-
- [1] M. C. Lagomarsino, C. Tanase, J. W. Vos, A. M. C. Emons, B. M. Mulder, and M. Dogterom, *Biophys. J.*, **92**, 1046 (2007).
- [2] D. N. Fuller, J. P. Rickgauer, P. J. Jardine, S. Grimes, D. L. Anderson, and D. E. Smith, *Proc. Natl. Acad. Sci. USA*, **104**, 11245 (2007).
- [3] N. Kleckner, D. Zickler, G. F. Jones, J. Dekker, R. Padmore, J. Henle, and J. Hutchinson, *Proc. Natl. Acad. Sci. USA*, **101**, 12592 (2004).
- [4] D. Bates and N. Kleckner, *Cell*, **121**, 899 (2005).
- [5] S. Jun and B. Mulder, *Proc. Natl. Acad. Sci. USA*, **103**, 12388 (2006).
- [6] Y. Liu and B. Chakraborty, arXiv:0906.4023 (2009).
- [7] P.-G. de Gennes, *Scaling concepts in polymer physics* (Cornell University Press, Ithaca, NY, 1979).
- [8] Y.-L. Chen, M. D. Graham, J. J. de Pablo, G. C. Randall, M. Gupta, and P. S. Doyle, *Phys. Rev. E*, **70**, 060901 (2004).
- [9] K. Jo, D. M. Dhingra, T. Odijk, J. J. de Pablo, M. D. Graham, R. Runnheim, D. Forrest, and D. C. Schwartz, *Proc. Natl. Acad. Sci. USA*, **104**, 2673 (2007).
- [10] D. J. Bonhuis, C. Meyer, D. Stein, and C. Dekker, *Phys. Rev. Lett.*, **101**, 108303 (2008).
- [11] H. Uemura, M. Ichikawa, and Y. Kimura, *Phys. Rev. E*, **81**, 051801 (2010).
- [12] J. O. Tegenfeldt, C. Prinz, H. Cao, S. Chou, W. W. Reisner, R. Riehn, Y. M. Wang, E. C. Cox, J. C. Sturm, P. Silberzan, and R. H. Austin, *Proc. Natl. Acad. Sci. USA*, **101**, 10979 (2004).
- [13] W. Reisner, K. J. Morton, R. Riehn, Y. M. Wang, Z. Yu, M. Rosen, J. C. Sturm, S. Y. Chou, and E. Frey, *Phys. Rev. Lett.*, **94**, 196101 (2005).
- [14] D. Stein, F. H. J. van der Heyden, W. J. A. Koopmans, and C. Dekker, *Proc. Natl. Acad. Sci. USA*, **103**, 15853 (2006).

- (2006).
- [15] M. Daoud and P.-G. de Gennes, *J. de Phys. France*, **38**, 85 (1977).
- [16] F. Brochard and P. G. de Gennes, *J. Phys. France Lett.*, **40**, 399 (1979).
- [17] Z.-G. Wang, A. M. Nemirovsky, and K. F. Freed, *J. Chem. Phys.*, **86**, 4266 (1987).
- [18] D. Romeis and Z. Usatenko, *Phys. Rev. E*, **80**, 041802 (2009).
- [19] J. H. van Vliet and G. ten Brinke, *J. Chem. Phys.*, **93**, 1436 (1990).
- [20] J. H. van Vliet, M. C. Luyten, and G. ten Brinke, *Macromolecules*, **25**, 3802 (1992).
- [21] S. Jun, D. Thirumalai, and B.-Y. Ha, *Phys. Rev. Lett.*, **101**, 138101 (2008).
- [22] Y. Jung, S. Jun, and B.-Y. Ha, *Phys. Rev. E*, **79**, 061912 (2009).
- [23] Cordeiro, Molisana, and Thirumalai, *J. Phys. II France*, **7**, 433 (1997).
- [24] D. W. Schaefer, J. F. Joanny, and P. Pincus, *Macromolecules*, **13**, 1280 (1980).
- [25] P. J. Flory, *Principles of Polymer Chemistry* (Cornell University Press, Ithaca, NY, 1953).
- [26] S. F. Edwards and P. Singh, *J. Chem. Soc. Faraday Trans.*, **75**, 1001 (1979).
- [27] G. Morrison and D. Thirumalai, *J. Chem. Phys.*, **122**, 194907 (2005).
- [28] M. Doi and S. F. Edwards, *The theory of polymer dynamics* (Oxford University Press, NY, 1994).
- [29] D. Frenkel and B. Smit, *Understanding molecular simulation: from algorithms to applications* (Academic press, NY, 2002).
- [30] G. S. Grest and K. Kremer, *Phys. Rev. A*, **33**, 3628 (1986).